Plagioclase crystal size distributions, growth and nucleation rates in an anhydrous arc basaltic andesite

Melvyn Billon[1*], Jacqueline Vander Auwera[1], Olivier Namur[2], François Faure[3], Marian B. Holness[4], Bernard Charlier[1]

Chemical Analysis

We performed EDS and WDS analyses (CAMECA SX Five Tactics at the LMV in Clermont-Ferrand, France; JEOL JXA-8530F at the Department of Material Engineering, KU Leuven, Belgium; and JEOL JXA-ISP 100 in Aachen, Germany) of glasses (using a defocused beam) and Fe-Ti oxides and plagioclase crystals. SEM imaging was performed at a working distance of 10–15 mm, with a dwell time of 10 µs and a voltage of 15 KV (20 KV for EDS analyses, with a beam current of 6–9 nA). Calibration details for WDS analyses are provided below. Up to 10–15 plagioclase crystals and 6–9 Fe-Ti oxides per sample were analyzed by WDS.

The CAMECA SX Five Tactics (Clermont-Ferrand) calibration standards were the same as those of Bechon et al. (2022): wollastonite (Ca, Si), $TiMnO_3$ (Ti, Mn), Al_2O_3 (Al), fayalite (Fe), forsterite (Mg), albite (Na,), Cr_2O_3 (Cr), orthose (K), and NiO (Ni). Experimental charges analyzed with this calibration were G 1-2 and G 1-4 (1 °C/h, 1140 °C and 1100 °C, respectively), G 2-1 and G 2-2 (3 °C/h, 1165 °C and 1140 °C, respectively), and G 3-1, G 3-2 (samples 1 and 2), G 3-3, and G 3-4 (9 °C/h, from 1165 °C to 1100 °C, respectively).

For the JEOL JXA-8530F (KULeuven), the standards were:

- Obsidian (SiO_2, Al_2O_3, K_2O), apatite (P_2O_5), diopside (CaO), hematite (FeO), jadeite (Na_2O), olivine (MgO), rutile (TiO_2), rhodonite (MnO), chromium oxide (Cr_2O_3), and nickel (NiO) for glasses.
- Albite (Al_2O_3), diopside (SiO_2), apatite (P_2O_5), hematite (FeO), jadeite (Na_2O), olivine (MgO), obsidian (K_2O), diopside (CaO), rutile (TiO_2), chromium oxide (Cr_2O_3), and rhodonite (MnO) for plagioclase.

The experimental charges analyzed with this calibration were G 0 (1190 °C during 24 h) and G 2-1 (3 °C/h, 1165 °C).

The standards for the JEOL JXA-ISP 100 (Aachen University) were:

- Glass (SiO_2, Al_2O_3, K_2O), jadeite (Na_2O), olivine (MgO), apatite (P_2O_5), diopside (CaO), rutile (TiO_2), hematite (FeO), Mn oxide (MnO), and chromite (Cr_2O_3) for glasses.
- Plagioclase (SiO_2, Al_2O_3, CaO), jadeite (Na_2O), olivine (MgO), apatite (P_2O_5), orthoclase (K_2O), rutile (TiO_2), hematite (FeO), Mn oxide (MnO), and chromite (Cr_2O_3) for plagioclase.
- Plagioclase (Al_2O_3), olivine (SiO_2, MgO), rutile (TiO_2), magnetite (FeO), Mn oxide (MnO), chromite (Cr_2O_3), and Ni oxide (NiO) for Fe-Ti oxides.

The experimental charges analyzed with this calibration were G 0 (1190 °C during 24 h), series G 1 (cooled at 1 °C/h), G 2-2, G 2-3, and G 2-4 (3 °C/h, 1140 °C, 1120 °C, and 1100 °C, respectively), and G 3-1, G 3-3b, G 3-5, and G 3-6 (9 °C/h, 1165 °C, 1120 °C, 1050 °C, and 1000 °C, respectively).

WDS analyses of plagioclase confirmed homogeneous anorthite contents (excluding cores of crystals corresponding to pre-existing crystals)) for each sample, with 1σ errors between 0.01 and 0.04 An mol.%. EDS analyses were more scattered, with 1σ errors between 0.01 and 0.08 wt.%. Crystals analyzed by both EDS and WDS exhibited differences in

anorthite content ranging from 1% to 13% (see ***Supplementary Material 2***). Glasses (quenched melt) were measured by WDS in some samples (up to eight analyses per sample) (***Supplementary Material 2***).

Crystal Size Distribution (CSD)

Theory

The theory of the CSD was initially developed by Randolph and Larson (1971), and later used in petrological context by Marsh (1988, 1998). This method is based on the conservation over time "*t*", of a magma volume "*V*" containing a crystal population density "*n*" within a size range "*ΔL*":

$$\frac{\partial(Vn)}{\partial t} + \frac{\partial(GVn)}{\partial L} = Q_i n_i - Q_0 n_0 \quad (1)$$

The evolution of the crystal population is governed by the rates at which new crystals nucleate "*J*" and growth "*G*"; as well as by the influx $(Q_i n_i \Delta L \Delta t)$ and outflux $(Q_0 n_0 \Delta L \Delta t)$ of crystals.

Another way to write this evolution is: $n(t) = \frac{dN}{dL} = (1 - \varphi(t)) \times \frac{J(t)}{G(t)}$ (2)

where *φ(t)* corresponds to the evolution of crystallinity with time, and "*N*" is the number of crystals with a size equal or less than "*L*".

In some magmatic systems, the variation in the total volume is often considered negligible:

$$\frac{\partial n}{\partial t} + \frac{\partial(Gn)}{\partial L} + \frac{n}{t} = 0 \quad (3)$$

and CSDs can be represented by the log-linear relation (see **Fig. 1**):

$$\ln(n) = \ln(n^0) - \frac{L}{Gt} \quad (4)$$

With the following parameters:

$$Intercept = \ln(n^0) \text{ at } L = 0 \quad (5)$$

$$slope = \frac{-1}{Gt} \quad (6)$$

$$J = \frac{dN}{dL_{L=0}} \times \frac{dL}{dt} = n^0 \times G \quad (7)$$

The slope of a CSD depends on both nucleation and growth rates.

Marsh's theory (1988, 1998) considered two endmembers: (a) crystallization in an open system, such as a magmatic chamber (or industrial crystallizers), from which crystals are removed once they reach a certain size; and (b) crystallization in a closed system, such as in experimental charges, where no crystals are removed.

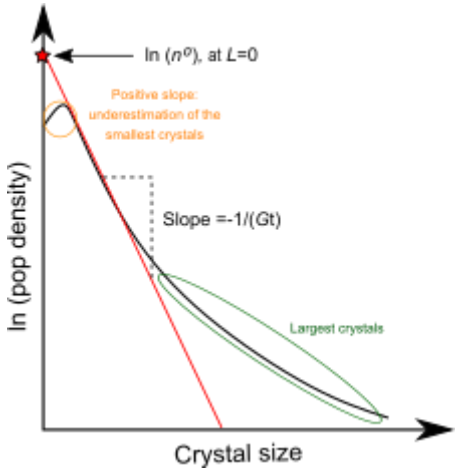

Fig. 1: Example of a typical CSD curve divided into three segments. The slope and intercept parameters from the linear regression (shown in red) are also indicated. The positive slope and flattened segment correspond to the smallest and largest crystals, respectively. These two regions are often attributed to inaccuracies in estimating the number of crystals for these size ranges. In the case of natural samples, they can also result from various magmatic processes.

(a) Crystallization in open system

In open systems such as magmatic chamber where crystals are continuously renewed, the volume of the system can be assumed to remain constant. At a steady state (time independent), with G supposed constant (independent of both time and crystal size), equation (3) becomes:

$$\frac{dn}{dL} = \frac{-1}{G\tau} \times n \quad (8)$$

We refind the log-linear relation (4). The nucleation rate "*J*" defined in the equation (7) is also constant in this case, with no influence on the CSD slope.

(b) Crystallization in a closed (Batch) system

In systems similar to experimental crystallization, the right term in equation (1) corresponding to the influx and outflux of crystals is zero, and crystallinity constantly increases with time:

$$\frac{\partial(Vn)}{\partial t} + G\frac{\partial(Vn)}{\partial L} = 0 \quad (9)$$

The general CSD profile is comparable to that in open system, and identical at the earliest stages of crystallization (Marsh, 1988). In a closed system, the negative slope of a CSD can result from two processes:

(i) An exponential increase of the nucleation rate (J) over time, at a constant growth rate (G). The CSD curve shifts upward along the nucleation density (Y) axis with a constant slope (C_j), independent of time (t) and crystal size (L).

$$J(t) = J_0 \exp(C_j \times t) \quad (10)$$

where J_0 and C_j are constants.

(ii) An exponential increase in the growth rate (G) with increasing crystal size (L), at a constant nucleation rate (J). This results in a curved CSD, where the y-intercept is governed by the nucleation, and the slope is equal to C_g. In this case, the characteristic crystal size (l_c) measuring crystallization time is not a linear relation between G and t.

$$G(L) = G_0 \exp(C_g \times L) \quad (11)$$

Where G_0 and C_g are constants.

Plots

Because it is not straightforward to estimate true 3D population densities from 2D sections, we compared CSDs generated using only the 2D major axis l (without 3D estimation) to those generated using the *CSDCorrections* method of Higgins (2000) to quantify the associated errors on derived nucleation and growth rates. To plot CSD profiles

along the real 3D axis *L*, the *CSDCorrections* assumes that all crystals have the same 3D shape. However, it is unlikely that all crystals in a sample have the same shape, particularly when multiple crystal generations coexist.

Here, we considered the 2D major axis (*l*) and an estimation of the 3D shape of the entire crystal population (i.e. the volumetric aspect ratio *S*:*I*:*L*), simulated using *ShapeCalc* Excel spreadsheet to simulate *L*. Plagioclase CSDs were calculated (***Supplementary Material 4***) using the 2D major axis, as in several other studies. Crystal sizes were estimated from BSE images (40–160× magnification). The total sample area, plagioclase abundance, and vesicularity (often <1%) were calculated using *Fiji* software. 3D CSDs were determined using Higgins' (2000) stereological conversion (CSDCorrections plugin). The CSDs were created on semi-logarithmic plots of the volumetric crystal density (N_V) normalized by the bin width (bw) vs. the 2D (*l*) or 3D (*L*: estimated with the CSDCorrections plugin) major axis length.

$$\text{For each size range } i,\ N_{V,i} = \frac{N_{A,i}}{S_{n,i}}. \quad (12)$$

As noted by Armienti (2008), CSDs depend on the number of size intervals used. Consequently, various size bin widths (*bw*) were compared: log 10; and *bw* = 5, 10, or 20 µm (***Supplementary Material 4***). The l_c, n_0, *J*, and *G* values (**Tables 4** and **5**) correspond to averages of the various data obtained with the different bin widths.

All CSDs had similar global shapes, but we noted that the slope of the CSDs varied for different size intervals in the case of the largest crystals. In particular, the CSDs plotted with a constant bin width showed truncation effects and a nearly horizontal slope for the largest crystals, because too few large crystals were available for inclusion (Higgins, 2000; Armienti, 2008).

References

Armienti P (2008) Decryption of Igneous Rock Textures: Crystal Size Distribution Tools. Reviews in Mineralogy and Geochemistry 69:623–649. https://doi.org/10.2138/rmg.2008.69.16

Higgins MD (2000) Measurement of crystal size distributions. American Mineralogist 85:1105–1116. https://doi.org/10.2138/am-2000-8-901

Marsh BD (1988) Crystal size distribution (CSD) in rocks and the kinetics and dynamics of crystallization. I. Theory. Journal of Petrology 99:277-291.

Marsh BD (1998) On the Interpretation of Crystal Size Distributions in Magmatic Systems. Journal of Petrology 39:553-599. https://doi.org/10.1093/petroj/39.4.553

Randolph AD, Larson MA (1971) Theory of particulate processes. Academic Press New York, 251 pp